Physica Scripta

PAPER • **OPEN ACCESS**

Calculation of shear viscosity in Au+Au collisions at NICA energies

Recent citations

- Shear viscosity of nucleons and pions in heavy-ion collisions at energies of NICA
E Zabrodin *et al*

To cite this article: E Zabrodin *et al* 2020 *Phys. Scr.* **95** 074009

View the article online for updates and enhancements.

This content was downloaded from IP address 84.209.32.239 on 08/03/2021 at 12:46

OPEN ACCESS
IOP Publishing
Physica Scripta
Phys. Scr. **95** (2020) 074009 (7pp)
https://doi.org/10.1088/1402-4896/ab9035

Calculation of shear viscosity in Au+Au collisions at NICA energies

E Zabrodin[1,2], M Teslyk[1,3], O Vitiuk[1,3] and L Bravina[1,2]

[1] Department of Physics, University of Oslo, PB 1048 Blindern, N-0316 Oslo, Norway
[2] Skobeltsyn Institute of Nuclear Physics, Moscow State University, RU-119991 Moscow, Russia
[3] Taras Shevchenko National University of Kyiv, UA-01033 Kyiv, Ukraine

E-mail: zabrodin@fys.uio.no

Received 2 March 2020, revised 28 April 2020
Accepted for publication 5 May 2020
Published 14 May 2020

International Conference on New Frontiers in Physics (ICNFP19)August 2019

Abstract

Shear viscosity of hot and dense nuclear matter, produced in the central zone of central gold-gold collisions at energies of NICA, is calculated within the UrQMD model. Besides the microscopic simulations of heavy ion collisions, the procedure assumes the application of statistical model to determine the temperature and chemical potentials in the system, and study of the relaxation process within the UrQMD box with periodic boundary conditions. The latter is used for calculation of the correlator which enters the Green-Kubo formula for shear viscosity. The fluctuations at early and late stages of the system evolution are studied. Results are compared to predictions of other models.

Keywords: relativistic heavy-ion collisions, microscopic transport model, box calculations, shear viscosity, Green-Kubo formalism

(Some figures may appear in colour only in the online journal)

1. Introduction

Experiments on heavy-ion collisions at relativistic and ultra-relativistic energies are the only means to study the properties of hot and dense nuclear matter in the laboratory. Analyzing the data obtained at RHIC (BNL) physicists came to the conclusion that the created substance possessed the properties of perfect fluid [1–4]. However, it became clear soon that one had to employ the nonzero shear viscosity η for the correct description of differential elliptic flow v_2 of hadrons as function of transverse momentum p_T within the framework of hydrodynamics. Recall, that the absolute minimum for the ratio of η to the entropy density s, η/s, estimated in the AdS-CFT formalism, equals $1/4\pi$ [5] in system of natural units, $c = \hbar = k_B = 1$. Hydrodynamic calculations use a bit higher values to describe the experimental data, i.e. $\eta/s = 0.12$ at RHIC for Au+Au collisions at $\sqrt{s} = 200$GeV, and 0.20 at LHC (CERN) for Pb+Pb collisions at $\sqrt{s} = 2.76$ TeV [6].

As was pointed out in [7], the ratio η/s reaches minimum in the vicinity of tricritical point for all known substances. It appears that at energies of LHC the phase transition between the quark-gluon plasma (QGP) and hadrons is a smooth crossover. The phase transition QGP−hadrons is expected to be of the first order at much lower energies accessible for beam energy scan (BES) at RHIC and future facilities NICA (JINR) and FAIR (GSI). The search for the tricritical point, where the first order phase transition becomes the second order one, is in the agenda of all experiments planned at the aforementioned accelerators. In the present work we would like to study the shear viscosity and its ratio to entropy density in the midrapidity range of central heavy-ion collisions at energies between $E_{lab} = 10$ and 40 AGeV generated by the microscopic transport model UrQMD [8, 9]. Note, that except of [10], η/s ratio was studied in various models for closed systems with fixed values of energy density and baryon density [11–22]. We are going to extend the results of [10], obtained within the equilibrium approach for calculation

Original content from this work may be used under the terms of the Creative Commons Attribution 4.0 licence. Any further distribution of this work must maintain attribution to the author(s) and the title of the work, journal citation and DOI.

 © 2020 The Author(s). Published by IOP Publishing Ltd Printed in the UK

of the entropy density, to the nonequilibrium case. The paper is organized as follows. Determination of shear viscosity by means of Green-Kubo approach is described in section 2. Section 3 presents the basic ingredients of model calculations including the UrQMD model, statistical model (SM) of an ideal hadron gas, and UrQMD box, which is a closed system. Results of our study obtained both with equilibrium and nonequilibrium entropy are discussed in section 4. Conclusions are drawn in section 5.

2. Determination of shear viscosity. Green-Kubo formalism

To determine the shear viscosity one usually employs the Green-Kubo method [23, 24]. It assumes the exponential damping of fluctuations whereas the closed system relaxes to equilibrium. The shear viscosity for the system with volume V and temperature T reads

$$\eta(t_0) = \frac{V}{T}\int_{t_0}^{\infty} \mathrm{d}t\,\langle \pi^{ij}(t)\pi^{ij}(t_0)\rangle_t, \tag{1}$$

where t_0 and t is the initial time and final time, respectively. The correlator in the integrand is

$$\langle \pi^{ij}(t)\pi^{ij}(t_0)\rangle_t = \lim_{t_{\max}\to\infty}\left[\frac{1}{t_{\max}}\int_{t_0}^{t_{\max}} \mathrm{d}t'\pi^{ij}(t+t')\pi^{ij}(t')\right]. \tag{2}$$

It contains the traceless parts of the energy-momentum tensor T^{ij}

$$\pi^{ij}(t) = \frac{1}{V}\sum_{k=1}^{N_{part}} \frac{p_k^i(t)p_k^j(t)}{E_k(t)}. \tag{3}$$

Here $p_k^{i(j)}(t)$ and $E_k(t)$ denote the $i(j)$-th components of momentum and energy of k-th particle. The sum in Eq.(3) runs over all particles. The correlator (2) should drop exponentially with time in the vicinity of equilibrium, therefore, it can be approximated by the exponential

$$\langle \pi^{ij}(t)\pi^{ij}(t_0)\rangle_t = \langle \pi^{ij}(t_0)\pi^{ij}(t_0)\rangle \exp\left(-\frac{t-t_0}{\tau}\right), \tag{4}$$

containing the effective relaxation time τ. Thus, to find the shear viscosity one has to determine both T and τ, because Eq.(1) is reduced to

$$\eta(t_0) = \tau\frac{V}{T}\langle \pi^{ij}(t_0)\pi^{ij}(t_0)\rangle. \tag{5}$$

Calculation of these parameters is explained in the next section.

3. Model setup

From the description of the method of shear viscosity extraction it becomes clear that we have to organize several steps to complete our task. First, while running the transport string model for heavy-ion collisions at given energy, we should determine the volume to search for local equilibrium. Previous studies reveal [25–28] that central cubic cell with volume $V = 5 \times 5 \times 5 = 125$ fm^3 is well suited for our analysis. But the cell is an open system and particles can leave it freely. The initially hot and dense fireball quickly expands, and its bulk characteristics are promptly changing. In order to investigate how far is the matter in the cell from local equilibrium one has to extract three basic parameters, namely, energy density ε, net baryon density ρ_B, and net strangeness density ρ_S, and insert it as an input to the statistical model of an ideal hadron gas. If the abundances of hadronic species and their energy spectra in the microscopic model calculations are close to those given by the SM, we can conclude that the matter is in the vicinity of chemical and thermal equilibrium. This procedure enables us to determine the temperature T, baryochemical potential μ_B, and the strangeness chemical potential μ_S. Finally, the behavior of the correlator $\langle \pi^{ij}(t)\pi^{ij}(t_0)\rangle_t$ in a system with fixed parameters ε, ρ_B, ρ_S should be studied. This can be done with the help of box with periodic boundary conditions to keep key system parameters constant. At this stage we get the value of shear viscosity at given T, μ_B, μ_S. The basic principles of the three stages are presented below.

3.1. Microscopic transport model

The UrQMD is formulated as Monte-Carlo event generator allowing to perform various analyzes of the measurable quantities by introducing all necessary experimental cuts. The model is designed to describe hadronic, hadron-nucleus, and nucleus-nucleus collisions in a broad energy range. In the hadronic sector UrQMD treats the production of new particles via formation and fragmentation of specific colored objects, strings. Strings are uniformly stretched, with constant string tension $\kappa \approx 1$ GeV/fm, between the quarks, diquarks and their antistates. The excited string is fragmenting into pieces via the Schwinger-like mechanism of $q\bar{q}$-pair production, and the produced hadrons are uniformly distributed in the rapidity space.

In contrast to models which rely on the color exchange mechanism of string excitation, like QGSM [29, 30] or NEXUS [31], the UrQMD model employs the longitudinal excitation of strings. Here the string masses arise from the momentum transfer. Tables of the experimentally available information, like hadron cross sections, resonance widths, their decay modes, and so forth are implemented. In case of lacking the information, the model employs the detailed balance considerations, the one-boson exchange model, and isospin symmetry conditions. The propagation of particles is governed by Hamilton equation of motion. Newly produced hadrons can interact further only after a certain formation time. The Pauli principle is taken into account via the blocking of the final state, if the outgoing phase space is occupied.

3.2. Statistical model of an ideal hadron gas

If the system is in thermal and chemical equilibrium, its macroscopic characteristics are fully determined by particle

distribution functions

$$f(p, m_i) = \left[\exp\left(\frac{\sqrt{p^2 + m_i^2} - \mu_B B_i - \mu_S S_i}{T}\right) \pm 1\right]^{-1}, \tag{6}$$

where p and m_i is the momentum and the mass of the hadron species i, respectively. Sign $-$ stands for bosons and $+$ for fermions. One has to know just three parameters, namely, temperature T and chemical potentials assigned to the conserved charges, i.e. baryon chemical potential $\mu_{\rm B}$ and strangeness chemical potential $\mu_{\rm S}$. Chemical potential of i-th hadron depends on its baryon and strangeness content, $\mu_i = B_i\mu_B + S_i\mu_S$. The dependence on chemical potential $\mu_{\rm Q}$ associated with electric charge is disregarded here, because $\mu_{\rm Q}$ is usually an order of magnitude weaker compared to $\mu_{\rm B}$ and $\mu_{\rm S}$. Then, the expressions for particle number density n_i, energy density ε_i and pressure P read

$$n_i = \frac{g_i}{2\pi^2}\int_0^\infty p^2 f(p, m_i)dp \tag{7}$$

$$\varepsilon_i = \frac{g_i}{2\pi^2}\int_0^\infty p^2\sqrt{p^2 + m_i^2}\, f(p, m_i)dp \tag{8}$$

$$P = \frac{g_i}{2\pi^2}\int_0^\infty p^2 dp\ \frac{p^2}{3(p^2 + m_i^2)^{1/2}} f(p, m_i). \tag{9}$$

with g_i being the spin-isospin degeneracy factor. The entropy density s_i can be calculated either from the Gibbs thermodynamic identity

$$Ts_i = \varepsilon_i + P_i - \mu_B\rho_{B_i} - \mu_S\rho_{S_i}, \tag{10}$$

or via the distribution function

$$s_i = -\frac{g_i}{2\pi^2}\int_0^\infty f(p, m_i)[\ln f(p, m_i) - 1]\, p^2 dp, \tag{11}$$

The total energy density ε, baryon density ρ_B and strangeness density ρ_S calculated microscopically within the cell at time t are inserted into the set of nonlinear equations

$$\varepsilon = \sum_i \varepsilon_i^{\rm SM}(T, \mu_B, \mu_S), \tag{12}$$

$$\rho_B = \sum_i B_i \cdot n_i^{\rm SM}(T, \mu_B, \mu_S), \tag{13}$$

$$\rho_S = \sum_i S_i \cdot n_i^{\rm SM}(T, \mu_B, \mu_S). \tag{14}$$

to determine temperature T, baryon chemical potential μ_B and strangeness chemical potential μ_S. After that all characteristics of the system in equilibrium are known and particle spectra can be compared with those obtained from microscopic model calculations.

3.3. Box for simulation of infinite nuclear matter

The standard choice for such a simulation is a cubic box with periodic boundary conditions [32–34] to ensure the energy and momentum conservation. If one particle leaves the box, another particle, fully identical to the first one, enters the box from the opposite side. The box should be neither too big nor too small, e.g. $V = 10 \times 10 \times 10 = 1000$ fm^3 [32] or $V = 5 \times 5 \times 5 = 125$ fm^3 [33]. The energy density ε, the net baryon density ρ_B, and the net strangeness density ρ_S are fixed at the initial stage. Recall, that for the infinite nuclear matter the net strangeness is zero, but for the central cell in relativistic heavy-ion collisions, which is an open system, ρ_S can differ from zero [25, 27]. In case of $\rho_S = 0$ the initial configuration in the box consists of protons and neutrons uniformly distributed in the configuration space. Their momenta are then rescaled to get the required energy density. If $\rho_S \neq 0$ certain admixture of kaons can be added. When the system is prepared, hadrons start to interact, and one can follow the microscopic model calculations to trace the system evolution and study the relaxation of hadron-string matter in the box to equilibrium.

4. Results

A bit more than 50.000 Au+Au collisions were generated at each of four bombarding energies. Figures 1(a)–(c) shows energy density, net baryon density, and net strangeness density obtained from the microscopic calculations in the central cell at times between 1 and 20 fm/c. Within first few fermiseconds the colliding nuclei fully overlap. This moment corresponds to highest energy density and baryon density in the fireball. The fireball expands, and both characteristics drop. Strangeness demonstrates another behavior. It is negative for all four energies. After reaching minimum, ρ_S is relaxing to zero at late times. This behavior is explained by domination of baryons over antibaryons in the cell. Therefore, according to [25–28], positive kaons can leave the cell earlier than negative kaons because of the smaller interaction cross sections, thus maintaining the negative though small net strangeness. Inserting the values of $\{\varepsilon, \rho_B, \rho_S\}$ as an input in the SM we obtain $\{T, \mu_B, \mu_S\}$ corresponding to equilibrated ideal hadron gas. Evolutions of these parameters are shown in figures 1(d)–(f). Since the matter in the cell at the very beginning is far from the equilibrium, one should treat the SM parameters obtained for earlier times with great care. Large baryon and energy densities observed at $t \leqslant 5$ fm/c are caused by interpenetration of two Lorentz-contracted nuclei, thus leading to very high temperatures of the hadron gas. Chemical and thermal equilibrium of nuclear matter in microscopic calculations in this energy range takes about 6-8 fm/c. After this time, as seen in figure 1(d), the temperature obtained at all four energies sit on the top of each other. Both chemical potentials tend to rise with decreasing energy of the collisions. However, μ_B in all cells increases with time, whereas μ_S decreases.

We are ready now to start the box calculations. Figure 2 shows correlators defined by equation (1) calculated for all four collision energies. The input data again are ε, ρ_B, ρ_S extracted from the central cell of Au+Au central collisions at times 1, 3, 6, 9, 12, 15, 18, and 20 fm/c after the beginning of the collision. The results of the box calculations are shown for times $t_{box} \geqslant 300$ fm/c, which are typical relaxation times of hot and dense nuclear matter in the box [33]. All correlators

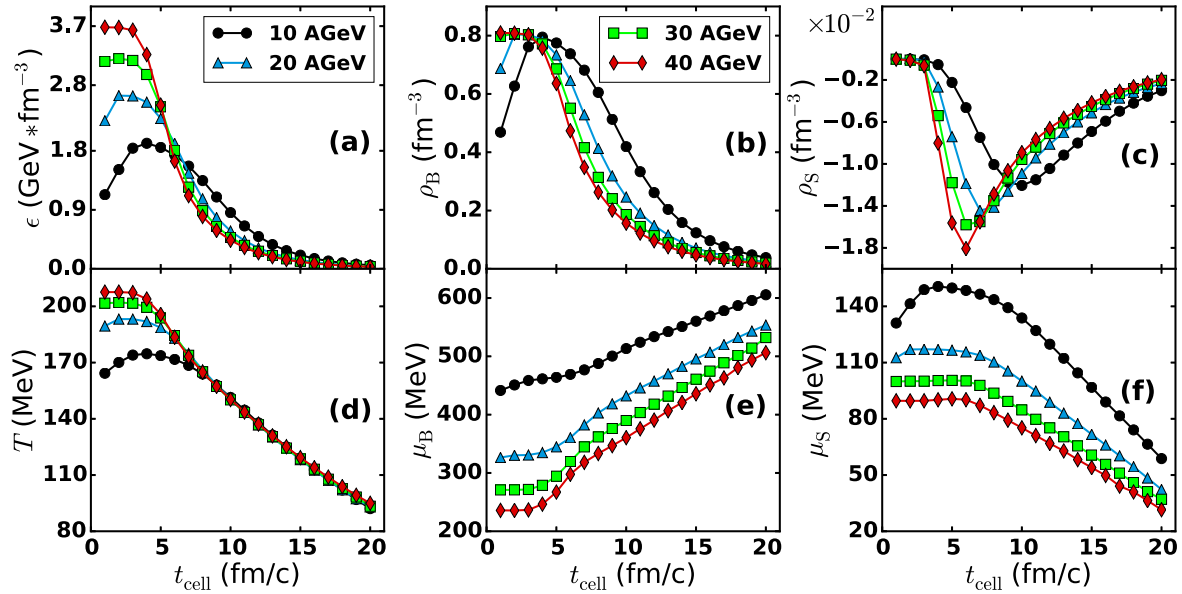

Figure 1. Time evolution of (a) energy density ε, (b) net baryon density ρ_B^{net}, (c) net strangeness density ρ_S^{net}, (d) temperature T_{SM}, (e) baryon chemical potential μ_B, and (f) strangeness chemical potential μ_S in the central cell with $V = 125$ fm^3 in central Au+Au collision calculated within UrQMD at energies $E_{lab} = 10$ AGeV (circles), 20 AGeV (triangles), 30 AGeV (squares), and 40 AGeV (diamonds). Lines are drawn to guide the eye.

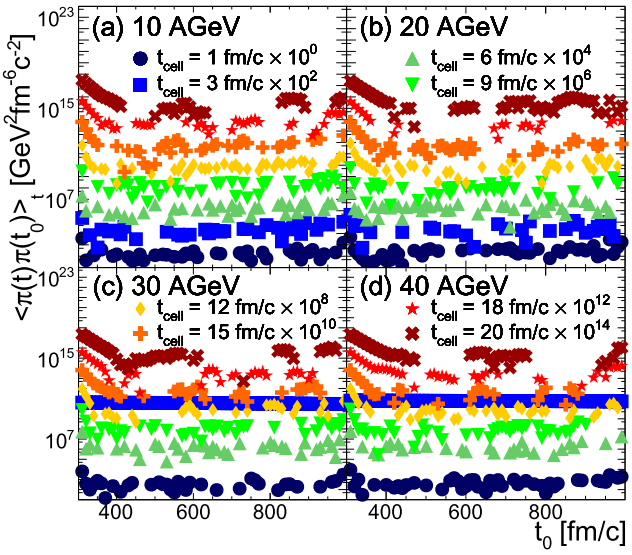

Figure 2. Correlators $\langle \pi(t)\pi(t_0)\rangle_t$ for initial cutoff time $t_0 = 300$ fm/c in the UrQMD box calculations. Initial conditions for the boxes are taken from the central cell with $V = 125$ fm^3 of Au+Au collisions at (a) $E_{lab} = 10$ AGeV, (b) 20 AGeV, (c) 30 AGeV, and (d) 40 AGeV at times $t = 1, 3, 6, 9, 12, 15, 18, 20$ fm/c. Each distribution is multiplied by its own factor 10^n.

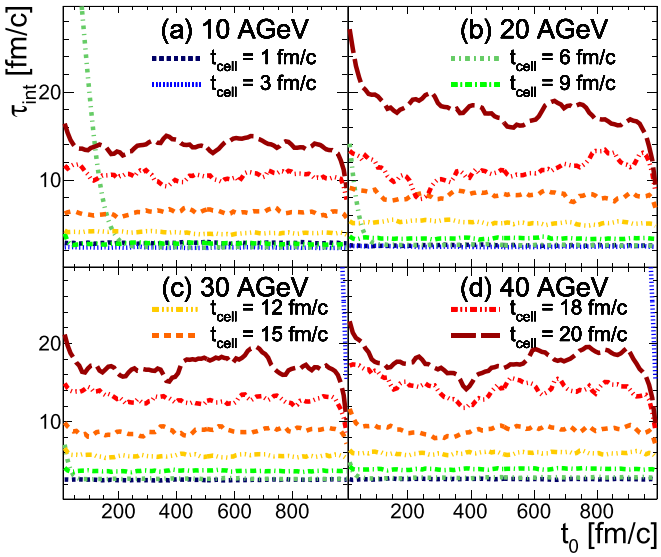

Figure 3. Relaxation time $\tau_{int}(t_0)$ for the collision energies (a) $E_{lab} = 10$ AGeV, (b) 20 AGeV, (c) 30 AGeV, and (d) 40 AGeV for the cell times $t_{cell} = 1, 3, 6, 9, 12, 15, 18, 20$ fm/c in the UrQMD box calculations.

reveal exponential falloff with time in accordance with equation (5). For few of them, corresponding to early cell times, the relaxation rates are significantly slower compared to those corresponding to late times. One can see such behavior in figure 2(c) and (d) for calculations with initial conditions similar to those at $t = 3$ fm/c in the central cell of central Au+Au collisions at $E_{lab} = 30$ and 40 AGeV. This occurs because of initialization of one (or two) very ultra-relativistic kaons. It takes quite long time to redistribute their energy and momenta among other particles in the box. The correlators appear to rise at late times. These momentum correlations arise because the UrQMD forces decay of all strongly decaying resonances at the end of the box calculations. Figure 3 displays the relaxation time τ_{int}, determined by means of equation (2), as function of the initial cutoff time t_0. The relaxation takes a longer period for t_0 shorter than 200 fm/c and vanishes for $t_0 \geqslant 900$ fm/c. For the initial times within the interval $200 \leqslant t_0 \leqslant 900$ fm/c the relaxation time is constant, except for very early cell times.

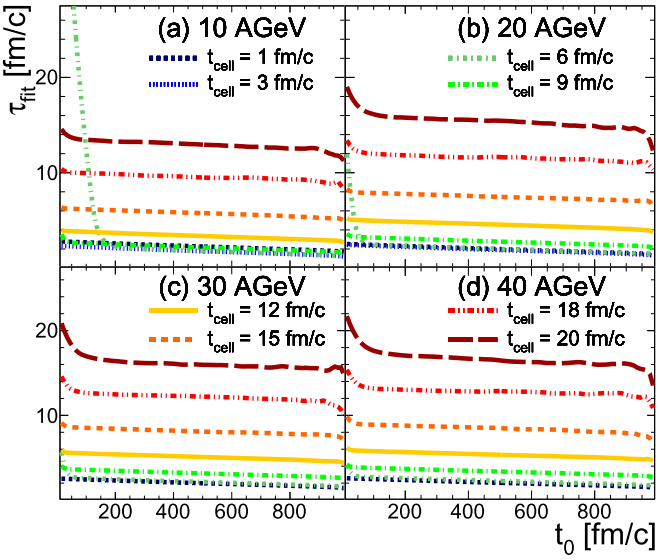

Figure 4. The same as figure 3 but for relaxation time $\tau_{\rm fit}(t_0)$.

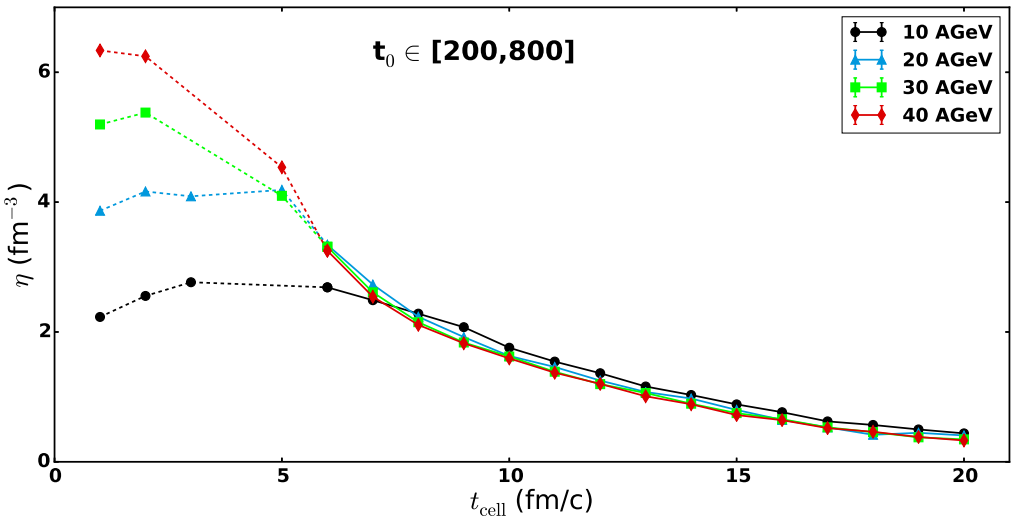

Figure 5. Shear viscosity $\eta(t_{\rm cell})$ of hadrons in the central cell of central Au+Au collisions at (a) $E_{lab} = 10$ AGeV, (b) 20 AGeV, (c) 30 AGeV, and (d) 40 AGeV within the UrQMD box calculations. Lines are drawn to guide the eye.

The behavior of $\tau_{\rm fit}$, obtained after fitting our results to equation (3), is presented in figure 4. It is very similar to that of $\tau_{\rm int}$, but it has no stochastic oscillations. Note that the distributions demonstrates some slope in the plateau region at $t_0 \geqslant 200$ fm/c as compared to the results shown in figure 3. This slope may somehow influence the determination of η values. Therefore, we average the value of $\tau_{\rm int\ (fit)}$ over the plateau in order to reduce statistical errors. Large values of the relaxation time $\tau_{\rm int(fit)}$ for some early cell times $t_{\rm cell}$ are explained by the abundant production of new particles and their rescattering in very hot and dense baryon-rich matter at the very beginning of the collision. Additional time delay is caused by the aforementioned single negative kaons. Combination of these factors leads to the extension of the box calculations up to 2000-2500 fm/c.

Results, obtained after averaging over the plateau, are displayed in figure 5. Note that the statistical errors are smaller than the symbol sizes. One can see that shear viscosity distributions for all four energies converge to each other at $t \approx 6$ fm/c. The matter in the cell becomes very dilute at the late times, and η drops almost to zero. This behavior is almost identical to the decrease of the cell temperatures seen in figure 1(d). Recall that the chemical potentials of net baryon charge and net strangeness are different, as shown in figure 1(e)-(f). It means that shear viscosity is predominantly determined by the temperature and not by μ_B and μ_S. The entropy density, however, does depend on both temperature and chemical potentials.

To show this we present in figure 6 the dependencies of ratio η/s on (a) time, (b) temperature, (c) baryon chemical potential, and (d) strangeness chemical potential for all four reactions in question.

The nonequilibrium stages of the system evolution are shown by dashed lines. We see that this ratio decreases with

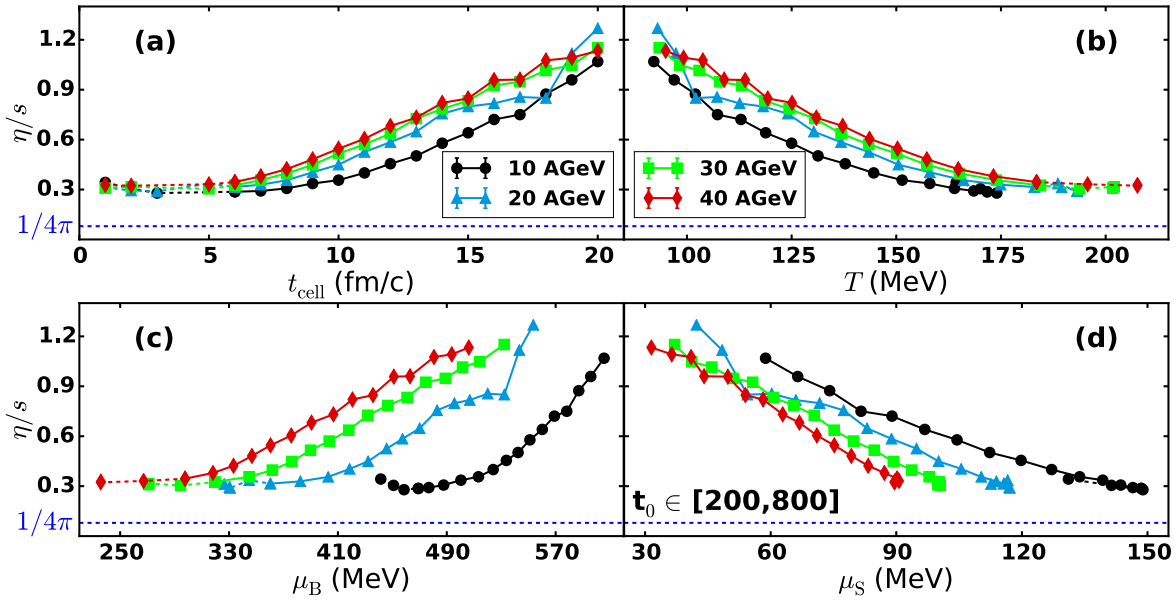

Figure 6. Shear viscosity to entropy ratio $\eta/s^{\rm sm}$ as function of (a) time t, (b) temperature T, (c) baryon chemical potential μ_B, and (d) strangeness chemical potential μ_S in the UrQMD calculations of central cell of central Au+Au collisions at $E_{lab} = 10$ AGeV (circles), 20 AGeV (triangles), 30 AGeV (squares), and 40 AGeV (diamonds). Lines are drawn to guide the eye.

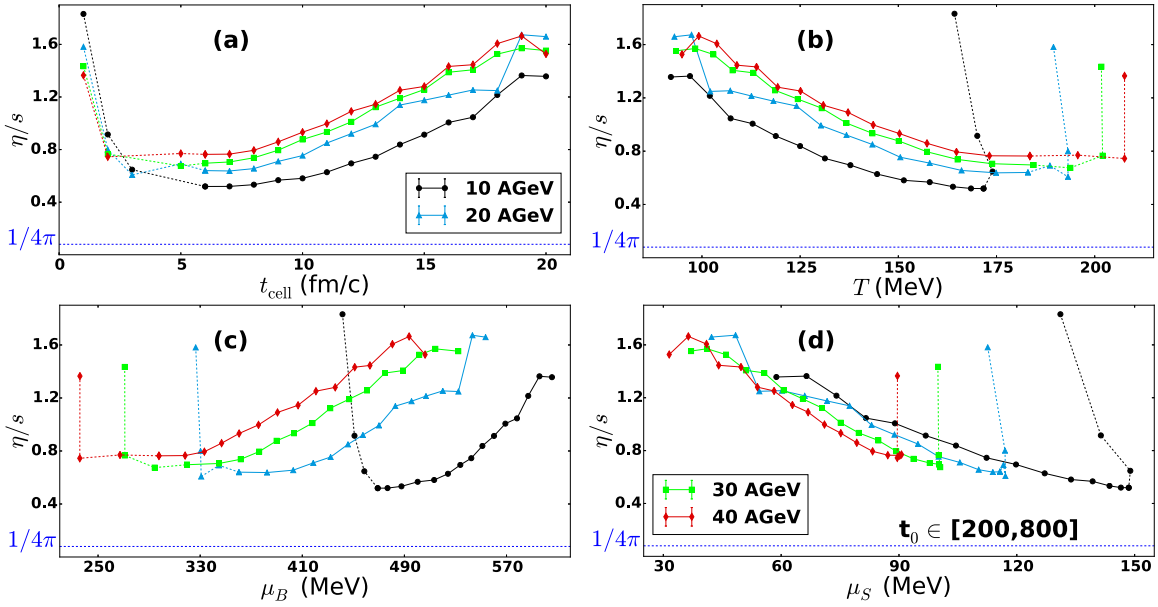

Figure 7. The same as figure 6 but for ratio of shear viscosity to nonequilibrium entropy density, η/s^{noneq}.

increase of the bombarding energy. Since the shear viscosity is almost the same, this circumstance implies the drop of entropy density with rising E_{lab}. It can be explained by faster loss of energy density in the central cell in case of more energetic collisions. Also, no distinct minima are observed. Recall, however, that we used the entropy density, calculated for the hadron gas in thermal and chemical equilibrium, even for the early stages of the collision when the matter in the cell was far from equilibrium. Obviously, the entropy density of nonequilibrated system should be lower than that of the equilibrated one. To estimate the nonequilibrium entropy, we insert in Eq. (11) instead of the equilibrium distribution functions (6) another ones provided by the hadron momentum distributions

$$f_i(p) = \frac{(2\pi)^3}{Vg_i}\frac{dN_i}{d^3p} \tag{15}$$

It is worth noting that the temperature at nonequilibrium stage is determined as average of partial temperatures of hadron species. Time evolution of η/s^{noneq} in the cell together with its dependencies on temperature, on baryon chemical potential, and on strangeness chemical potential are shown in figure 7. Here the minima for all four energies are clearly seen. This occurs at time $t \approx 5 - 6$ fm/c corresponding to maximum baryon density in the system. The lower the

bombarding energy, the deeper the minimum in of η/s distribution. The study should be extended to lower energies in order to see where the ratio of shear viscosity to entropy density will stop to decrease. We are in the energy region where the equation of state (EOS) is expected to be changed because of the formation of non-hadronic objects, quark-gluon strings.

5. Conclusions

The self-consistent procedure for determination of shear viscosity and its ratio to entropy density within the microscopic model calculations is developed. It includes three steps. First, we define the volume in A + A collisions to look for the local equilibrium. This is a very important condition, because the Green-Kubo formalism employed for determination of shear viscosity implies the relaxation of out-of-equilibrium matter to the equilibrated state. The central cubic cell with volume $V = 125$ fm^3 is well suited for our analysis. Second, we extract the energy density, net baryon density, and net strangeness density out of the tested volume. The procedure is repeated with the time step $\Delta t = 1$ fm/c. The extracted values are inserted into a system of non-linear equations of the statistical model of an ideal hadron gas with essentially the same number of degrees of freedom, as in the microscopic model. This allows one to determine temperature, baryon chemical potential, and strangeness chemical potential in the tested volume in case the hadron yields and energy spectra, calculated micro- and macroscopically, are close to each other. Finally, the values of T, μ_B, μ_S are used to initialize the box with periodic boundary conditions in the framework of the same microscopic transport model. Here the Green-Kubo formalism is applied to determine η, ratio η/s, and so forth.

The developed procedure was used to study the shear viscosity of hot and dense nuclear matter in the central zone of central gold-gold collisions at energies $E_{lab} = 10$, 20, 30 and 40 AGeV, accessible for BES, NICA, and FAIR facilities. For calculations we employ the UrQMD model. We found that, for all four tested energies, the temperatures and shear viscosities are very close to each other after 5-6 fm/c. Both T, η and s in the cell drop with time, whereas the ratios η/s, however, reach minima at $t \approx 5$ fm/c, irrespective of the bombarding energy. Then the ratios rise until the very late stages of the system evolution. The minima in η/s become more pronounced if the nonequilibrium entropy density is used. The rise of η/s is accompanied by the simultaneous increase of baryon chemical potential and decrease of both temperature and strangeness chemical potential in the cell.

Acknowledgments

The work of L B and E Z was supported by the Norwegian Research Council (NFR) under Grant No. 255 253/F50 - 'CERN Heavy Ion Theory' and by the Russian Foundation for Basic Research (RFBR) under Grants No. 18-02-40084 and No. 18-02-40085. M T and O V acknowledge financial support of the Norwegian Centre for International Cooperation in Education (SIU) under Grant 'CPEA-LT-2016/10094—From Strong Interacting Matter to Dark Matter'. All computer calculations were made at Abel (UiO, Oslo) and Govorun (JINR, Dubna) computer cluster facilities.

ORCID iDs

M Teslyk https://orcid.org/0000-0001-6311-4679

References

[1] BRAHMS Collaboration, Arsene I *et al* 2005 *Nucl. Phys.* A **757** 1
[2] PHOBOS Collaboration, Back B B *et al* 2005 *Nucl. Phys.* A **757** 28
[3] STAR Collaboration, Adams J *et al* 2005 *Nucl. Phys.* A **757** 102
[4] PHENIX Collaboration, Adcox K *et al* 2005 *Nucl. Phys.* A **757** 184
[5] Kovtun P, Son D T and Starinets A O 2005 *Phys. Rev. Lett.* **94** 111601
[6] Schenke B, Tribedy P and Venugopalan R 2012 *Phys. Rev. Lett.* **108** 252301
Schenke B, Tribedy P and Venugopalan R 2012 *Phys. Rev.* C **86** 034908
[7] Csernai L P, Kapusta J I and McLerran L D 2006 *Phys. Rev. Lett.* **97** 152303
[8] Bass S A *et al* 1998 *Prog. Part. Nucl. Phys.* **41** 255
[9] Bleicher M *et al* 1999 *J. Phys. G: Nucl. Part. Phys.* **25** 1859
[10] Teslyk M *et al* 2020 *Phys. Rev.* C **101** 014904
[11] Muronga A 2004 *Phys. Rev.* C **69** 044901
[12] Demir N and Bass S A 2009 *Phys. Rev. Lett.* **102** 172302
[13] Chakraborty P and Kapusta J I 2011 *Phys. Rev.* C **83** 014906
[14] Wesp C *et al* 2011 *Phys. Rev.* C **84** 054911
[15] Cremonini S 2011 *Mod. Phys. Lett.* B **25** 1867
[16] Noronha-Hostler J *et al* 2012 *Phys. Rev.* C **86** 054902
[17] Ozvenchuk V *et al* 2013 *Phys. Rev.* C **87** 064903
[18] Karpenko Iu A *et al* 2015 *Phys. Rev.* C **91** 064901
[19] Ivanov Yu B and Soldatov A A 2016 *Eur. Phys. J.* A **52** 117
[20] Rais J, Gallmeister K and Greiner C 2019 *The shear viscosity to entropy density ratio in Hagedorn states* arXiv:1909.04522 [hep-ph]
[21] Rose J B *et al* 2018 *Phys. Rev.* C **97** 055204
[22] Motornenko A *et al* 2018 *J. Phys. G: Nucl. Part. Phys.* **45** 035101
[23] Green M S 1954 *J. Chem. Phys.* **22** 398
[24] Kubo R 1957 *J. Phys. Soc. Japan* **12** 1957
[25] Bravina L V *et al* 1998 *Phys. Lett.* B **434** 379
[26] Bravina L V *et al* 1999 *J. Phys. G: Nucl. Part. Phys.* **25** 351
[27] Bravina L V *et al* 1999 *Phys. Rev.* C **60** 024904
[28] Bravina L V *et al* 2008 *Phys. Rev.* C **78** 014907
[29] Amelin N S and Bravina L V 1990 *Sov. J. Nucl. Phys* **51** 133
[30] Bleibel J, Bravina L V and Zabrodin E E 2016 *Phys. Rev.* D **93** 114012
[31] Drescher H J *et al* 2001 *Phys. Rept* **350** 93
[32] Belkacem M *et al* 1998 *Phys. Rev.* C **58** 1727
[33] Bravina L V *et al* 2000 *Phys. Rev.* C **62** 064906
[34] Bratkovskaya E L *et al* 2000 *Nucl. Phys.* A **675** 661